Обчислювальний експеримент в матеріалознавстві

UDC 620.178.1:539.533 https://doi.org/10.15407/materials2021.03.013

Extended characterization of materials based on continuous instrumented indentation diagrams

B. A. Galanov, S. M. Ivanov*, V. V. Kartuzov

I.M. Frantsevich Institute for Problems of Materials Science of the NAS of Ukraine
Ukraine, 03142, Kyiv, Kzhyzhznovsky str., 3
*E-mail: ism@ipms.kiev.ua

In addition to the traditional determination of hardness and elastic moduli from continuous diagrams of instrumental indentation, it is proposed to determine the yield stress, the characteristic of plasticity, the characteristic relative size of the elastoplastic zone under the indenter, and the volumetric deformation of the material in the area of contact of the indenter with the sample. The indentation diagram shows the transition point to the unconstrained material flow under the indenter.

Keywords: *indentation, hardness, elastic moduli, contact stiffness, elastic-plastic strains.*

Introduction

At present, the instrumented indentation technique [1, 2] is widely used to determine the hardness and elastic moduli of materials [1, 2], which uses a continuous recording of the experimental indentation diagram (P—h), where P is the force acting on the indenter, h is the approach of the indenter and the sample. The basis of this technique are the functional theoretical relations between P and, h which are obtained for the unloading branch of the diagram (P—h) from the known solutions of the elastic contact problem, and were proposed in the 70s of the last century by Bulychev, Alekhin and Shershorov [3, 4] for use in the instrumental indentation method in determining hardness and elastic moduli of materials. This proposal became decisive for the subsequent development and improvement of the technique of measuring hardness and elastic moduli with instrumental indentation devices [5—12] with continuous recording of diagrams (P—h) on a wide scale of forces P and displacements h.

The application and improvement of this technique also revealed its shortcomings, limitations and difficulties of use, which were analyzed,

discussed and compared with other methods in numerous works [1—12], where various corrections (including corrections obtained experimentally) were proposed to the theoretical relations. Some systematic critical analysis of these problems is given in [2]. There have been attempts to take into account in the basic relations of the method [1, 2] the elastic deformation of indenters, the imperfection of their geometry, and other factors [1, 2, 5—10].

The critical analysis performed in [12] revealed errors in the method of instrumental determination of hardness and elastic moduli [1, 2] and insufficient substantiation of some of its provisions.

This circumstance served as the motivation for the present work, devoted to a deeper critical revision and extension of the basic functional theoretical relations of this method, which expanded the list of the determined properties of materials. Based on the indentation model [13], the technique is supplemented by: determination of the yield stress of the sample material, the characteristic size of the elastic-plastic zone under the indenter and the point of the beginning of the unconstrained flow of the material under the indenter on the indentation diagram. These refinements, additions and proposals are made without invoking additional (to the hypotheses [1, 2]) assumptions and experimental measurements. The results are illustrated by examples of application and improvement of the proposed methodology.

Analysis of the Oliver-Pharr methodology and comments to it

The widely used Oliver-Pharr method [1, 2] for determining the hardness HM and effective Young's modulus E^* is based on the use of experimental values of the maximum pressing force $P_{\max}$, the corresponding maximum approach $h_{\max}$ of the indenter and the sample, and the elastic stiffness of the indenter and the sample $S = \dfrac{dP}{dh}$, which are measured on the unloading branch of the continuous indentation diagram (P—h) at $P = P_{\max}$ and $h = h_{\max}$ (Fig. 1). The method assumes that the contact surface of the indenter and the flat surface of the sample after deformation are of the same type as the surface of the indenter: spherical if the indenter has a spherical surface; conical if the indenter has a conical surface; pyramidal if the indenter has a pyramidal surface, etc. After unloading, which is assumed to be elastic, the surfaces of the indenter and the sample in the contact region have the same property, i.e., they are surfaces of the same type as the indenter and touch at the same point at the beginning of reloading.

In Fig. 2 for the unloading branch shown in Fig. 1, an explanatory computational scheme of the elastic contact of the indenter (with the surface $z = h_f - r\cot\gamma_i$) and the indentation (with the surface $z = h_f - r\cot\gamma_{SR}$) is presented. This diagram shows the values h_e, h_S, h_C as well as an equivalent absolutely rigid indenter with the surface $z = h_{\max} - r\cot\alpha$, $\cot\alpha = \cot\gamma_i - \cot\gamma_{SR}$, embedded in an elastic half-space $z > h_f$ with the boundary $z = h_f$ and an effective elastic modulus $E^* = \left(\dfrac{1-\nu_i^2}{E_i} + \dfrac{1-\nu_S^2}{E_S}\right)^{-1}$,

where E_i, ν_i, E_S, ν_S are the Young and Poisson moduli of the indenter (*i*) and the sample (*S*), respectively. The quantities h_S, h_C are the components of the elastic approach $h_e = h_S + h_C = h_C/(2\pi)$, the meaning of which is explained in Fig. 2.

With an elastic contact of the Hertz type, there is a constant relation between the quantities h_S, h_C [14]: $h_S/h_C = (\pi-2)/2$ $\left(h_S = 2(\pi-2)P_{\max}/(\pi S),\ h_C = 4P_{\max}/(\pi S)\right)$. The value $g(r) = r\cot\alpha$ is equal to the gap between the conical surfaces of the indentation and the indenter, touching their vertices at the point O' on the *z* axis after unloading. The quantity *a* is the radius of the elastic contact region after the subsequent loading of the indenter and the indentation by the force $P_{\max}$, and which is assumed to be equal to the indentation radius when the average contact pressure under the indenter is equal to the hardness *HM*. Therefore, this radius is equal to the radius of the contact area of the indenter with the sample under the force $P = P_{\max}$ and $h = h_{\max}$ (Fig. 1) after the first loading of the sample. As in the Hertz problem, elastic tangential displacements (parallel to the plane $z = 0$) are not taken into account, due to their smallness compared to vertical displacements (in the direction of the axis *z*).

The theoretical formula for the unloading branch of the diagram (*P*—*h*) obtained on the basis of the solution of an elastic contact problem of the Hertz type [14, 15] (Fig. 1 and 2), has the form

$$P = \frac{2}{\pi(\cot\gamma_i - \cot\gamma_{SR})} E^* \left(h - h_f\right)^2, \quad h_f \le h \le h_{\max}\ . \tag{1}$$

Elastic stiffness of this branch:

$$\frac{dP}{dh} = \frac{4}{\pi(\cot\gamma_i - \cot\gamma_{SR})} E^* \left(h - h_f\right). \tag{2}$$

If we denote $S = \left.\frac{dP}{dh}\right|_{h=h_{\max}}$, then from (1), (2), after excluding the value $\cot\alpha = \cot\gamma_i - \cot\gamma_{SR}$, for the elastic component of the approach of the indenter and the sample $h_e = h_{\max} - h_f$ we have

$$h_e = h_{\max} - h_f = 2P_{\max}/S\,. \tag{3}$$

Here the value $S = \left.\frac{dP}{dh}\right|_{h=h_{\max}} = 2E^* a$ is the experimentally measured value of the elastic stiffness of the unloading branch of the curve (*P*—*h*) [1, 2] (Fig. 1). Taking into account (1) and (3), for the quantity $\cot\alpha = \cot\gamma_i - \cot\gamma_{SR}$ we obtain

$$\cot\alpha = \frac{8}{\pi}\frac{P_{\max}}{S^2} E^*, \tag{4}$$

and the unloading branch (Fig. 1) is also represented by the following functional dependence:

$$P=\left(\frac{S}{2}\right)^2 P_{\max}^{-1}\left(h-h_{\max}+\frac{2P_{\max}}{S}\right)^2, \tag{5}$$

$$\frac{dP}{dh}=\frac{S^2}{2P_{\max}}\left(h-h_{\max}+\frac{2P_{\max}}{S}\right), \quad \left.\frac{dP}{dh}\right|_{h=h_{\max}}=S,$$

which uses only experimentally measured values $P_{\max}$, $h_{\max}$ and S and the assumption of elastic unloading.

Such *a priori* representation of the unloading branch, in essence, regularizes the definition of S by the formulas [12]

$$S=\frac{\sum_{i=1}^{N}\delta_i\left(1-\bar{P}_i^{1/2}\right)}{\sum_{i=1}^{N}\delta_i^2}>0, \quad \sum_{i=1}^{N}\delta_i^2\neq 0,\ \delta_i=\frac{\left(h_{\max}-h_i\right)}{2P_{\max}}\geq 0, \quad \bar{P}_i=\frac{P_i}{P_{\max}}, \tag{6}$$

where $\left(h_i, P_i=P\left(h_i\right)\right)$, $i=1,2,3,.....,N$ are the experimental values, which are the coordinates of the points of the unloading branch or its part (Fig. 1).

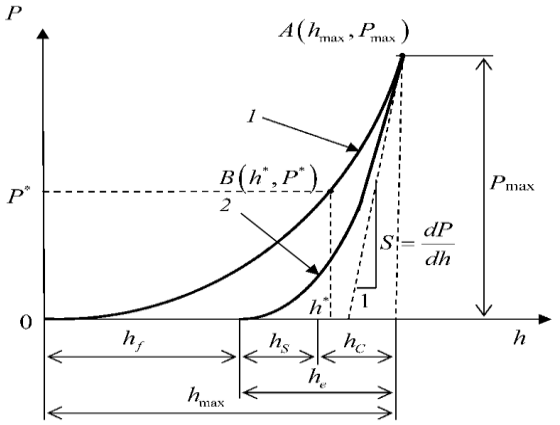

Fig. 1. $P(h)$ dependency diagram: sections of loading (1) and unloading (2) of the indenter; h_f is the indentation depth (Fig. 2); $h_e = 2P_{\max}/S$ is the elastic component of the approach of the indenter and the sample. $B(h^*, P^*)$ is the point of transition to unconstrained material flow under the indenter (see (13).

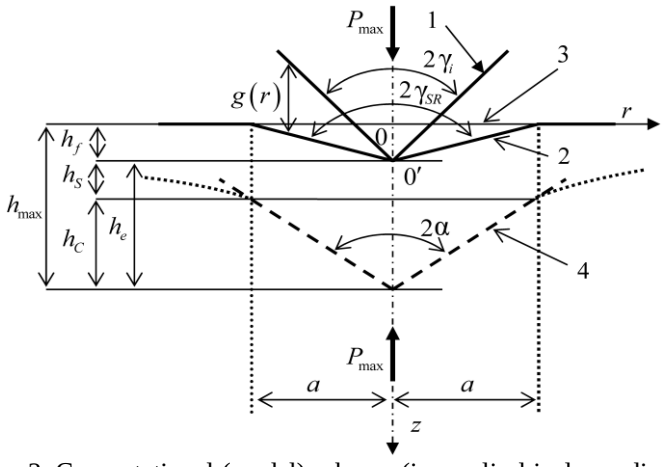

Fig. 2. Computational (model) scheme (in a cylindrical coordinate system $0r\varphi z$) of the introduction of an elastic conical indenter 1 into indentation 2; 3 is the initial surface of the sample $z=0$; 4 is the absolutely rigid equivalent indenter.

Thus, the stiffness S value determined by formula (6) continuously depends on the experimental data for the $P(h)$ dependence and is stable to their small changes. Note that the value S in the method [1, 2] is determined by the "continuous stiffness measurement" (CSM) technique using small dynamic oscillations imposed on forces (or displacements). The use of this technique to the one-sided contact of the indenter and the sample requires additional justification, due to the significant difference in the stiffness of one-sided bonds during their loading and unloading during oscillations.

Determination of the effective elastic modulus E^* and hardness HM

Relation (1) allows the following parametric representation [11, 14, 15]:

$$\begin{cases} P = \dfrac{\pi}{2} E^* a^2 \cot\alpha, \\ h = a\cot\alpha, \end{cases} \tag{7}$$

where the radius of the contact area a is a parameter.

From this and by the definition of the quantities h_S, h_C and $g(r)$ we have the equalities

$$h_e = h_S + h_C,\ h_S = \left(\frac{\pi}{2} - 1\right) h_C,\ h_C = g(a) = a\cot\alpha,\ h_e = \frac{\pi}{2} a\cot\alpha = \frac{\pi}{2} h_C. \tag{8}$$

Taking into account (4), for the quantity $\cot\gamma_{SR}$ in the equation of the indent surface $z = h_f - r\cot\gamma_{SR}$ we have

$$\cot\gamma_{SR} = \cot\gamma_i - \cot\alpha = \cot\gamma_i - \frac{8}{\pi}\frac{P_{\max}}{S^2} E^*, \tag{9}$$

and, since $0 = h_f - a\cot\gamma_{SR}$, for the radius of the imprint we have $a = \dfrac{h_f}{\cot\gamma_{SR}}$.

Hence, using the well-known relation $S = 2E^* a$, to determine the value of E^* we have the equation

$$\cot\gamma_{SR} = \frac{2h_f}{S} E^* = \cot\gamma_i - \frac{8}{\pi}\frac{P_{\max}}{S^2} E^*, \tag{10}$$

from which for the elastic modulus E^* and hardness $HM = \dfrac{P_{\max}}{\pi a^2}$ we obtain the formulas

$$E^* = S\frac{\cot\gamma_i}{2\left[h_{\max} + \left(\dfrac{4-2\pi}{\pi}\right)\dfrac{P_{\max}}{S}\right]},\quad HM = \frac{P_{\max}\cot^2\gamma_i}{\pi\left[h_{\max} + \left(\dfrac{4-2\pi}{\pi}\right)\dfrac{P_{\max}}{S}\right]^2}, \tag{11}$$

where $\dfrac{HM}{E^*} = \dfrac{2\cot\gamma_i}{\pi\left[1 + 2\left(\dfrac{2-\pi}{\pi}\right)\dfrac{P_{\max}}{Sh_{\max}}\right]}\dfrac{P_{\max}}{Sh_{\max}}$, and $P_{\max}, h_{\max}, S$ are values determined from the experimental indentation diagram (P—h).

Note that since the elastic modulus E^* does not depend on the plastic properties of the material, formula (11) should practically not depend (or "weakly" depend) on the choice of a point $A\left(h_{\max}, P_{\max}\right)$ on the indentation diagram (Fig. 1), that is, calculations with it must be stable with respect to the position of this point with experimental data: $\left(h_{\max}, P_{\max}, S\right)$. Elementary algebraic transformations can show that formulas (11) are another, simpler, form of the corresponding formulas in [12] and, therefore, they give the same results as the formulas in this work.

Determination of the yield point Y_S, the characteristic relative size of the elastoplastic zone $x = b_S/a$, and the volumetric deformation of the material ε_S in the region of contact of the indenter with the sample

The estimation of the yield stress and the size of the elastoplastic zone under the indenter is carried out on the basis of the indentation model [13], the scheme of which is given in Fig. 3. If the elastic characteristics of the sample and indenter material (E_S, ν_S, E_i, ν_i), as well as the hardness *HM* are known (or determined by formulas (11)), then the system of transcendental equations for determining the yield stress Y_S and the characteristic relative size of the elastoplastic zone $x = b_S/a \geq 1$ has the form [13]:

$$\begin{cases} \left(1+\varepsilon_S\right)\left(x^3 - \dfrac{2\left(1-2\nu_S\right)}{3\left(1-\nu_S\right)}\right) = \dfrac{E_S \cot\psi}{6\left(1-\nu_S\right)Y_S}, \\ HM = Y_S\left(\dfrac{2}{3} - \dfrac{\cot\psi}{\left(1+\varepsilon_S\right)}\ln\left[1 - \dfrac{\cot\psi}{2\left(1+\varepsilon_S\right)}\right] + 2\ln x\right), \\ \varepsilon_S = -\dfrac{3\left(1-2\nu_S\right)\left(HM - 2Y_S \ln x\right)}{E_S}, \end{cases} \tag{12}$$

whose solution with respect to real unknown quantities (x, Y_S) approximately determines the stress-strain state in the sample and the Tabor constant $C = HM/Y_S$ (see the second equation of system (12)). Here the value 2ψ determines the value of the angle at the top of the loaded conical indenter (Fig. 3) and $\cot\psi = \cot\gamma_i - 2\left(1-\nu_i^2\right)HM/E_i$.

Unfortunately, in the methodology [1, 2] for determining hardness *HM* and effective Young's modulus E^*, there are no *a priori* recommendations for choosing a point $A\left(h_{\max}, P_{\max}\right)$ on the diagram (*P*—*h*) when plastic deformations are sufficiently developed (that is, there is no criterion for sufficient development of plastic deformations). It seems that such *a priori* recommendations are difficult to define. In this regard, the *a posteriori* assessments of the force $P^* < P_{\max}$ gain importance when an unrestrained plastic flow under the indenter begins.

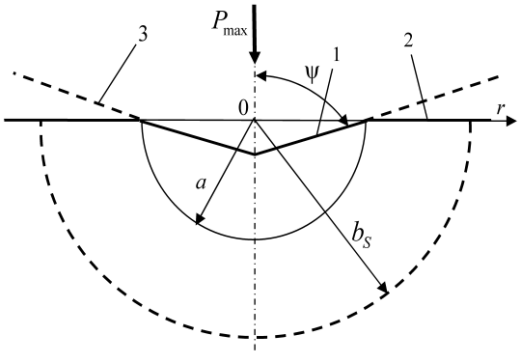

Fig. 3. Model scheme (in a spherical coordinate system with center 0) of zones under the indenter with different stress-strain states of the sample material: $r \le a$ is the hydrostatic core; $a < r \le b_S$ is the area of elastoplastic deformation; $r > b_S$ is the area of elastic deformation: 1 — conical contact surface of the indenter and the sample; 2 — sample surface; 3 — indenter under load with apex angle 2Ψ.

Based on the model [13], the contact radius a_0 and the force P^* acting on the indenter, at which an unconstrained plastic flow begins under the indenter, *a posteriori* are estimated, respectively, by the formulas

$$a_0 = a\left(1-\frac{\cot\psi}{2\left(1+\varepsilon_S\right)}\right), \quad P^* = \frac{a_0^2}{a^2}P_{\max} = \left(1-\frac{\cot\psi}{2\left(1+\varepsilon_S\right)}\right)^2 P_{\max}. \quad (13)$$

Force $P^* < P_{\max}$ corresponds to the approach $h = h^*$, determined from the diagram (*P*—*h*) (see Fig. 1).

Remark 1. *The above results are presented for the case of penetration of a cone with an apex angle* $2\gamma_i$*. The transition from pyramidal indenters to an equivalent conical one (and vice versa) can be performed using the condition of equality of the projection areas of the imprints left by different indenters with the same penetration volume (the same penetration depth for pyramidal and conical indenters). This condition leads to the following relationship between the tapering angles of equivalent conical, pyramidal (three- and four-faced) indenters:*

$$\cot\gamma_i = \frac{\sqrt{\pi}}{2}\cot\gamma_V = \sqrt[4]{\frac{\pi^2}{27}}\cot\gamma_B,$$

where γ_i, γ_V, γ_B are the tip angles of indenters: conical, tetrahedral (for example, Vickers, $\gamma_V = 68°$) and trihedral (for example, Berkovich, $\gamma_B = 65°$), respectively.

Remark 2. *In (12), it is assumed that the Poisson's ratio of the sample* ν_S *is known and is determined in tests independent (for example, by acoustic methods) from the experimental diagram (P—h) (Fig. 1).*

Plasticity characteristic δ_H and representative deformation ε_r

The magnitude of the plasticity characteristic δ_H is determined by the formulas [16, 17]

$$\delta_H = \varepsilon_p/\varepsilon_t,\ \varepsilon_t = \ln\sin\gamma_B, \varepsilon_p = \varepsilon_t - \varepsilon_e < 0, \varepsilon_e = -\left(1+\nu_S\right)\left(1-2\nu_S\right)HM/E_S, \quad (14)$$

where $\varepsilon_e, \varepsilon_p, \varepsilon_t$ are, respectively, elastic, plastic and total average in the contact area linear (in the direction of the force *P*, see Fig. 2) deformations, $\gamma_B = 65^o$.

The contact area refers to that part of the flat surface of the specimen that comes into contact with the indenter after deformation. In formulas (14), the quantity $\varepsilon_t = \ln\sin\gamma_B \approx -0.098$, $\gamma_i = 65°$ is constant and is determined by the *geometry of the contacting bodies (indenter and sample) before their deformation*. If for sufficiently developed plastic deformations we neglect the material compressibility (volumetric deformation $\varepsilon_{11} + \varepsilon_{22} + \varepsilon_{33} = 0$), then the value ε_t = −0,098 determines with good accuracy the average linear compressive deformation in the contact area in the direction of the force that acts on the indenter (Fig. 2), similar to uniaxial tension-compression. Therefore, this value can be considered as a representative (characteristic) deformation under uniaxial compression, as suggested by Tabor and Johnson [15]. This deformation corresponds to both the yield strength Y_S in Table 2 and the hardness value $HM = CY_S$, as the average value of the contact pressure under the indenter. In this case, the value of C is determined by the complex bulk stress-strain state of the sample under the indenter, which differs significantly from uniaxial compression. The structure of a representative deformation $\varepsilon_r = \varepsilon_e + \varepsilon_p$ is approximately estimated by the formula

$$\varepsilon_e = (1-\delta_H)\varepsilon_r, \ \varepsilon_p = \delta_H\varepsilon_r. \tag{15}$$

If the average total linear deformation and its components in the contact area of the indenter and the sample are determined from the *deformed* scheme in accordance with the formulas [17]

$$\varepsilon_t = \varepsilon_e + \varepsilon_p, \ \varepsilon_p = -\ln\sqrt{1+\cot^2\gamma_{SR}} < 0, \ \cot\gamma_{SR} = \cot\gamma_i - 2HM/E^*, \tag{16}$$

$$\varepsilon_e = -(1+\nu_S)(1-2\nu_S)\frac{HM}{E_S}, \ \frac{1}{E^*} = \frac{1-\nu_i^2}{E_i} + \frac{1-\nu_S^2}{E_S}, \ \bar{\delta}_H = \varepsilon_p/\varepsilon_t < \delta_H,$$

where $2\gamma_{SR}$ is the angle at the apex of the residual indentation in the sample after unloading the conical indenter, ε_e, ε_p, ε_t are, respectively, elastic, plastic and total average over the contact area, linear (in the direction of force P, see Fig. 2) deformations, then the value of ε_t will not be the same (constant) for all materials. However, as shown in [13], its average value $\langle\varepsilon_t\rangle = -0.060$ (for a large group of materials when indenting with a diamond Vickers indenter) has a small standard deviation $\sigma = 0.003$ and is almost constant. Formulas (16), in fact, are analogs of the formulas that determine the longitudinal deformation of a bar from its enlarged cross section under uniaxial compression.

Examples of determination of elastic moduli, hardness of materials, yield stress and characteristic size of the elastoplastic zone under the indenter

To validate the obtained relations, samples of fused silica FS and a single crystal of tungsten (111) W with a purity of 99,99% (material with a high shear modulus) were tested. The tests were carried out with a Nano Indenter G200 nanohardness tester with a diamond $(E_i = 1141$ ГПа, $\nu_i = 0.07)$ Berkovich indenter ($\gamma_B = 65°$) at loads of $P_{\max} = 97$ and 193 mN.

T a b l e 1. Experimental data for indentation for single crystal (111) tungsten (W) and fused silica (FS) [12]

Sample	P_{max}	h_{max}	S (6)
	P^* (13)	h^*	
	mN	mN	MN/m
W1	97	970	1.742
	66	745	
W2	193	1410	2.350
	130	1074	
FS1	97	898	0.3065
	61	695	
FS2	193	1289	0.399
	119	986	

The test results (P_{max}, h_{max}, S values for formulas (11)) are taken from [12], where their detailed description is given. Experimental diagrams of indenter penetration for fused silica and tungsten obtained at loads P_{max} = 97 and 193 mN are shown in Fig. 4. The complete theoretical unloading branches of the diagrams, constructed according to formula (1), are also given here.

The calculation results according to the proposed method using the test data are shown in Table 2. It is known that the elastic modulus of tungsten is 409 GPa, and that of fused quartz is 72 GPa. The modulus of elasticity for fused silica using our technique turned out to be markedly higher than 72 GPa. Perhaps this is a consequence of the fact that when the indenter penetrates the fused quartz, the material is compacted (about 20% [12]) in the contact zone, $\varepsilon_S \in [-0.19, -0.17]$ (Table 1).

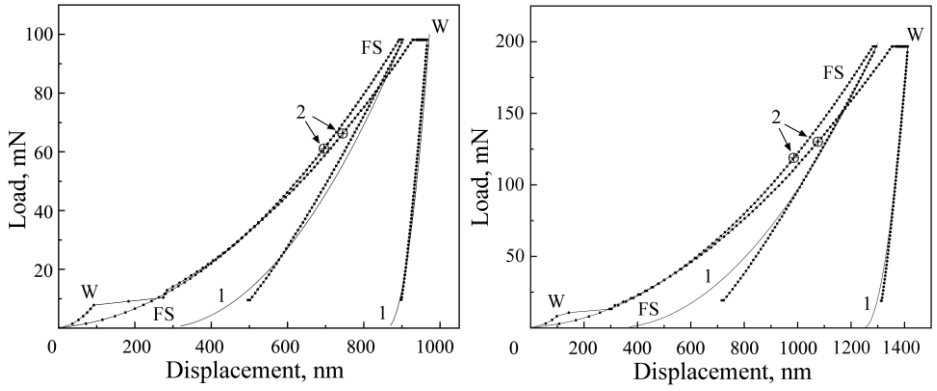

Fig. 4. Diagram of penetration of the Berkovich indenter for fused quartz and single crystal (111) tungsten: P_{max} = 97 (*a*) and 193 mN (*b*): 1 — unloading branch of diagrams, eq. (1) [12]; 2 — point (P^*, h^*) of the beginning of unconstrained plastic flow under the indenter (Table 1).

T a b l e 2. Results of calculations for nanoindentation of fused silica FS (ν_s = 0.17) and (111) plane of a tungsten single crystal W (ν_s = 0.28)

Sample	E^*, GPa (11)	HM, GPa (11)	E_s, GPa	b_s/a (12)	$\bar{\delta}_H$ (16)	δ_H (14)	Y_s, GPa (12)	C	ε_S (12)
W1	340	4.70	445	2.81	0.900	0.940	1.67	2.81	–0.0037
W2	316	4.43	401	2.76	0.895	0.937	1.60	2.77	–0.0039
FS1	83	9.10	87	1.08	0.113	0.180	9.82	0.93	–0.1707
FS2	77	9.19	80	1.06	0.080	0.102	10.25	0.90	–0.1947

Conclusions

An extended characterization of materials based on experimental continuous diagrams of instrumental indentation is proposed, which includes the determination of the following properties: moduli of elasticity, hardness, yield stress, characteristic size of the elastoplastic zone under the indenter, volumetric compressibility of the material under the indenter, characteristic of plasticity, representative deformation and its structure. *A posteriori*, the position of the point (on the experimental indentation diagram) of the beginning of the unconstrained flow of the material under the indenter was estimated.

References

1. Oliver, W. C., Pharr, G. M. (1992). An improved technique for determining hardness and elastic modulus using load and displacement sensing indentation experiments. J. Mater. Res., Vol. 7, No. 6, pp. 1564—1583. https://doi.org/10.1557/JMR.1992.1564
2. Oliver, W. C., Pharr, G. M. (2004). Measurement of hardness and elastic modulus by instrumented indentation: Advances in understanding and refinements to methodology. J. Mater. Res., Vol. 19, No. 1, pp. 3—20. https://doi.org/10.1557/jmr.2004.19.1.3
3. Bulychev, S. I., Alekhin, V. P., Shorshorov, M. K., Ternovskii, A. P., Shnyrev, G. D. (1975). Determination of Young's modulus according to indentation diagram. Industrial Laboratory, Vol. 41, pp. 1409—1412.
4. Shorshorov, M. K., Bulychev, S. I., Alekhin, V. P. (1981). Work of plastic and elastic deformation during indenter indentation. Soviet Physics - Doklady, Vol. 26, pp. 769—771.
5. Firstov, S. A., Gorban', V. F., Pechkovskii, E. P. (2009). Novaya metodologiya obrabotki i analiza rezul'tatov avtomaticheskogo indentirovaniya materialov. New methodology for processing and analyzing the results of automatic indentation of materials. Kyiv: Logos, 83 p. [in Russian].
6. Hay, J. C., Bolshakov, A., Pharr, G. M. (1999). A critical examination of the fundamental relations used in the analysis of nanoindentation data. J. Mater. Res., Vol. 14, No. 6, pp. 2296—2305. doi: https://doi.org/10.1557/JMR.1999.0306
7. Veprek, S., Mukherjee, S., Mannling, H.-D., He, J. (2003). On the reliability of the measurements of mechanical properties of superhard coatings. Mater. Sci. and Engineering, Vol. A 340, pp. 292—297. doi: https://doi.org/10.1016/S0921-5093(02)00195-8
8. Cao, Y. P., Dao, M., Lu, J. (2007). A precise correcting method for the study of the superhard material using nanoindentation tests. J. Mater. Res., Vol. 22, No. 5, pp. 1255—1264. doi: https://doi.org/10.1557/jmr.2007.0150

9. Veprek-Heijman, M. G. J., Veprek, R. G., Argon, A. S., Parks, D. M., Veprek, S. (2009). Non-linear finite element constitutive modeling of indentation into super- and ultrahard materials: The plastic deformation of the diamond tip and the ratio of hardness to tensile yield strength of super- and ultrahard nanocomposites. Surface & Coat. Techn, Vol. 203, pp. 3385—3391. doi: https://doi.org/10.1016/j.surfcoat.2009.04.028
10. Hay, J. L., Pharr, G. M. (2000). Instrumented Indentation Testing. ASM Hand¬book. Vol. 8: Mechanical Testing and Evaluation, 10th Edition, ASM International, Materials Park, OH., pp. 232—243. https://doi.org/10.31399/asm.hb.v08.a0003273
11. Borodich, F. M. (2014). The hertz-type and adhesive contact problems for depth-sensing indentation. Adv. Appl. Mechanics, Vol. 47, Burlington: Academic Press, pp. 225—366. doi: https://doi.org/10.1016/B978-0-12-800130-1.00003-5
12. Galanov, B. A., Dub, S. N. (2017). Critical Comments to the Oliver-Pharr Measurement Technique of Hardness and Elastic Modulus by Instrumented Indentations and Refinement of Its Basic Relations. J. of Superhard Mater., Vol. 39, No. 6, pp. 373—389. doi: https://doi.org/10.3103/S1063457617060016
13. Galanov, B. A., Ivanov, S. M., Kartuzov, V. V. (2020). Improved core model of the indentation for the experimental determination of mechanical properties of elastic-plastic materials and its application. Mechanics Mater., Vol. 150, pp. 103545. doi: https://doi.org/10.1016/j.mechmat.2020.103545
14. Sneddon, I. N. (1948). Boussinesq's Problem for a Rigid Cone. Proc. Cambridge Philos. Soc., Vol. 44, pp. 492—507. https://doi.org/10.1017/S0305004100024518
15. Johnson, K. L. (1985). Contact Mechanics. Cambridge: Cambridge University Press, 452 p. https://doi.org/10.1017/CBO9781139171731
16. Milman, Y. V., Galanov, B. A., Chugunova, S. I. (1993). Plasticity characteristic obtained through hardness measurement. Acta Metall. Mater., Vol. 41, pp. 2523—2532. doi: https://doi.org/10.1016/0956-7151(93)90122-9
17. Galanov, B. A., Milman, Y. V., Chugunova, S. I., Goncharova, I. V. (1999). Investigation of mechanical properties of high-hardness materials by indentation. J. Superhard Mater., Vol. 21, pp. 23—35.

Розширена характеризація матеріалів на основі безперервних діаграм інструментального індентування

Б. О. Галанов, С. М. Іванов*, В. В. Картузов

Інститут проблем матеріалознавства імені І. М. Францевича НАН України
*E-mail: ism@ipms.kiev.ua

Критично переглядаються основні функціональні теоретичні співвідношення методу інструментального визначення твердості і пружних модулів, які розширюють список визначуваних властивостей матеріалів. Додатково (до традиційного визначення твердості та пружних модулів за неперервними діаграмами інструментального індентування) пропонується визначати границю течії, характеристику пластичності, характерний відносний розмір пружнопластичної зони під індентором, об'ємну деформацію матеріалу в області контакту індентора із зразком. Наведено практичну методику розрахунку властивостей. Результати ілюструються прикладами застосування запропонованої вдосконаленої методики. Діаграма індентування показує точку переходу до необмеженої течії матеріалу під індентором.

Ключові слова: *індентування, твердість, модулі пружності, контактна жорсткість, пружнопластичні деформації.*